JOURNAL OF VIROLOGY, Feb. 2005, p. 2528–2540 Vol. 79, No. 4
0022-538X/05/$08.00+0 doi:10.1128/JVI.79.4.2528–2540.2005

Mutational Analysis of Narrow Pores at the Fivefold Symmetry Axes of Adeno-Associated Virus Type 2 Capsids Reveals a Dual Role in Genome Packaging and Activation of Phospholipase A2 Activity

Svenja Bleker, Florian Sonntag, and Jürgen A. Kleinschmidt*

Tumor Virology, German Cancer Research Center, Heidelberg, Germany

Received 30 July 2004/Accepted 3 November 2004

Adeno-associated virus type 2 (AAV2) capsids show 12 pores at the fivefold axes of symmetry. We mutated amino acids which constitute these pores to investigate possible functions of these structures within the AAV2 life cycle. Mutants with alterations in conserved residues were impaired mainly in genome packaging or infectivity, whereas few mutants were affected in capsid assembly. The packaging phenotype was characterized by increased capsid-per-genome ratios. Analysis of capsid-associated DNA versus encapsidated DNA revealed that this observation was due to reduced and not partial DNA encapsidation. Most mutants with impaired infectivity showed a decreased capability to expose their VP1 N termini. As a consequence, the activation of phospholipase A2 (PLA2) activity, which is essential for efficient infection, was affected on intact capsids. In a few mutants, the exposure of VP1 N termini and the development of PLA2 activity were associated with enhanced capsid instability, which is obviously also deleterious for virus infection. Therefore, PLA2 activity seems to be required on intact capsids for efficient infection. In conclusion, these results suggest that the pores at the fivefold axes function not only as portals for AAV2 single-stranded DNA packaging but also as channels for presentation of the PLA2 domain on AAV2 virions during infection.

The viral capsid can be considered as a multiprotein complex which not only protects the viral genome against extreme environmental influences outside the cell but also combines a number of functional elements which are needed for host cell recognition, intracellular trafficking, and disassembly in order to successfully deliver genetic information to the host cell (for reviews, see references 23, 60, and 75). These functional elements either are concomitantly transported with the virion as separate proteins or are part of the structural proteins themselves. Identifying such functional elements on viral capsids is one of the most attractive goals of viral structural research. Over the past few years, several such functional domains have been identified in parvoviruses (for a review, see reference 70).

Adeno-associated virus (AAV) type 2 (AAV2) is a member of the parvovirus family. AAV2 requires coinfection with helper viruses, such as adenovirus or herpesvirus, for efficient reproduction (4, 9, 58) and has a nonenveloped icosahedral capsid. It encloses a 4.7-kb single-stranded DNA (ssDNA) genome containing two large open reading frames, *rep* and *cap* (61). The Rep proteins, encoded by the *rep* gene, are required for DNA replication, DNA encapsidation, and control of gene expression (36, 45). The viral capsid is composed of three structural viral proteins (VPs), designated VP1, VP2, and VP3, which are encoded by the *cap* open reading frame and expressed from the p40 promoter. Capsids are formed with the VPs in an approximate molar ratio of 1:1:10 due to alternative splicing and an unconventional start codon for VP2. This ratio is also maintained in assembled capsids (6, 34). The VPs share common central and C-terminal regions with N-terminal extensions of 65 amino acids for VP1 and VP2 and an additional 138 N-terminal amino acids which form the unique portion of VP1.

Capsids of parvoviruses have a diameter of 18 to 26 nm and contain 60 copies of their capsid proteins, arranged with T = 1 icosahedral symmetry (84). Capsid structures of various parvoviruses have been resolved by X-ray crystallography or electron cryomicroscopy (1, 2, 3, 37, 40, 42, 59, 66, 71, 79, 83, 84). All of these particles show similar structural arrangements at the inner surface. The organization of the outer surface shows many differences. However, common features are a dimple-like depression at the twofold symmetry axes, three elongated spikes surrounding the threefold axes (except for B19), and 12 narrow pores at the fivefold axes. The precise localization of the N-terminal regions of VP1 and VP2 has not been determined in the structures resolved so far. There is evidence in some parvoviruses that the N termini of capsid proteins can protrude into the pores at the fivefold axes. In mature minute virus of mice (MVM) virions, the channels contain additional, weakly X-ray-dense material (40). Analysis of DNA-containing capsids of canine parvovirus (CPV) following refinement to 2.9 Å supports the assumption that this weak density represents peptide sequences of N termini of about 13% of the capsid proteins (83). A highly conserved glycine-rich sequence within the N termini of the VPs of MVM could be modeled into the weak density found along the pores (3). In empty CPV, MVM, and AAV2 capsids, the N-terminal regions are not accessible to antibodies (15, 37, 69); in AAV2, they are most likely located at the twofold axes inside the capsids (37). The N termini of VP2 in CPV and MVM capsids become at least partially accessible to antibodies or trypsin digestion upon DNA packaging (14, 15, 49, 67, 74). The exposure of VP1 N termini has been achieved in vitro by treatment with heat or urea (10, 15, 69). It was suggested that the unique N-terminal region of VP1

* Corresponding author. Mailing address: Tumor Virology, German Cancer Research Center, Im Neuenheimer Feld 242, 69120 Heidelberg, Germany. Phone: 49 6221 424978. Fax: 49 6221 424962. E-mail: J.Kleinschmidt @dkfz.de.

of CPV became exposed in vivo at the stage of cell entry within lysosomal vesicles (62); however, it was not clear whether the capsids were still intact or had already been dissociated.

AAV2 capsids enter the host cell in vitro by binding to heparan sulfate proteoglycan as a primary receptor and human fibroblast growth factor receptor 1 or αVβ5-integrin as a coreceptor (50, 63, 64). Internalization takes place by clathrin-mediated endocytosis followed by transport to the perinuclear area via endosomal pathways (5). A low pH seems to be required for endosomal escape either from early (5, 82) or from late (26) endosomes, which is necessary for successful infection. Some evidence suggests that even intact virus particles can enter the cell nucleus (5, 27, 54, 56, 82). However, if these particles brought about a productive AAV2 infection, then the final uncoating reaction would have to take place in the nucleus. Recently, it was reported that incubation of AAV2 virions in detergent-containing nuclear extracts from mouse liver led to the release of viral DNA from capsids, supporting this possibility (65). The unique N-terminal region of VP1 of autonomous parvoviruses, such as MVM or CPV, contains four basic clusters which are thought to control the nuclear import of incoming virions (41, 69). It is not clear whether similar sequences within the portion unique to VP1 and the portions common to VP1 and VP2 of AAV capsid proteins have the same function.

A conserved phopholipase A2 (PLA2)-like domain located at the unique region of VP1 of most parvoviruses plays an important role in viral infectivity (17, 22, 86). PLA2 activity is thought to be required between the stage of perinuclear accumulation of virions and the stage of early gene expression (22, 39, 86). Injection of VP1-specific antibodies into the cytoplasm of cells prior to inoculation with CPV prevented infection, suggesting that this domain is accessible to antibody recognition within the cytoplasm (69). Intact capsids show no PLA2 activity; however, for CPV and porcine parvovirus, it has been demonstrated that PLA2 activity can be induced in vitro by treatment with heat or acidic pH (62, 86).

The assembly of AAV2 has been described to occur through the introduction of strand-displaced single-stranded genomes into preformed capsids (46). It has been proposed that ssDNA is targeted to capsids by Rep proteins, which not only are able to bind specifically to inverted terminal repeats but also are found to form complexes with capsids (19). The helicase activity of the small Rep proteins is required to translocate full-length DNA into capsids (36). Neither the binding site of the Rep proteins on the capsid surface nor the channels through which the DNA could be introduced into capsids have been characterized so far.

The aim of this study was to characterize the role of the narrow pores at the fivefold symmetry axes of AAV2 capsids. Therefore, various mutants were generated by site-directed mutagenesis to contain alterations in pore-forming amino acids. Few mutants were impaired in capsid assembly. Other mutants exhibited an altered packaging phenotype characterized by increased capsid-per-genome ratios. However, most striking was a distinct reduction in infectivity observed for several mutants. These mutants were analyzed for their ability to externalize the N termini of VP1, thereby displaying PLA2 activity and possibly other domains required for viral infectivity. Our results showed that most infection-defective mutants were impaired in their ability to expose the VP1 N termini on intact capsids, resulting in inefficient activation of their PLA2 activity. Some mutants with impaired infectivity were characterized by enhanced capsid instability. Taken together, our data support the conclusion that the pores at the fivefold symmetry axes may function during virus assembly as channels for ssDNA encapsidation and during infection as channels for presentation of the PLA2 domain required for infectivity.

MATERIALS AND METHODS

Plasmids and site-directed mutagenesis. The construct pTAV2.0 (28) contains the entire AAV2 genome from pAV-2 (38), including both inverted terminal repeats, cloned into the BamHI site of Bluescript II. Plasmid pTAV2.1 is based on pTAV2.0. It contains a mutated Rep52/40 translation start site to prevent the expression of the small Rep proteins (36). Plasmid pJ407 (35) was used as a template for site-directed mutagenesis reactions. It contains the BamHI-NotI fragment of pTAV2.0 cloned into pUC131. Mutagenesis was performed by using a QuickChange site-directed mutagenesis kit (Stratagene, Amsterdam, The Netherlands) according to the manufacturer's recommendations. Two complementary PCR primers were designed for each mutant to contain a substitution, deletion, or insertion flanked by 10 to 15 homologous base pairs on each side of the mutation. The mutated plasmids were identified by DNA sequencing. The SwaI-BsiWI fragment containing the mutation was subcloned into the pTAV2.0 backbone. The complete fragment was sequenced to identify additional mutations.

Transfection of 293T cells and preparation of virus supernatants. Cells were used to seed 10-cm dishes at a density of 1.5×10^6 cells in 10 ml of Dulbecco's modified Eagle's medium (DMEM)–10% fetal calf serum (FCS) 1 day prior to transfection. Transfection by calcium phosphate precipitation was carried out with 12 μg of plasmid DNA per dish at 37°C (47). At 16 h posttransfection, the medium was removed and replaced with fresh medium containing adenovirus type 5 (Ad5) (multiplicity of infection [MOI], 2). Cells were incubated at 37°C for an additional 2 days, harvested, washed once with phosphate-buffered saline (PBS), and lysed by three rounds of freezing-thawing (−80°C and 37°C) in TNEM buffer (0.15 M NaCl, 50 mM Tris, 1 mM EDTA, 5 mM MgCl [pH 8.0]). Lysates were incubated at 56°C for 30 min to inactivate adenovirus. Cell debris was removed by centrifugation at $1,000 \times g$ for 20 min.

Large-scale production and purification of virus. Large-scale production of virus was performed by using twenty 15-cm dishes for transfection. A total of 4×10^6 cells in 20 ml of DMEM–10% FCS were used to seed each dish 1 day prior to transfection with 50 μg of DNA per dish. At 16 h posttransfection, the medium was replaced with medium containing Ad5 (MOI, 2). Cells were incubated at 37°C for an additional 2 days, harvested, washed once with PBS, and lysed by three rounds of freezing-thawing (−80 °C and 37°C) in 20 ml of PBS containing 1 mM $MgCl_2$ and 2.5 mM KCl (PBS-MK). Lysates were incubated at 56°C for 30 min to inactivate adenovirus and digested with Benzonase (200 U/ml; Sigma, Munich, Germany) for 30 min at 37°C. Cell debris was removed by centrifugation at $1,000 \times g$ for 20 min, and supernatants were loaded onto an iodixanol step gradient (7 ml of 15% iodixanol in PBS-MK–0.5 M NaCl and 5 ml of 25% iodixanol, 4 ml of 40% iodixanol, and 4 ml of 60% iodixanol in PBS-MK) in Beckman Quickseal tubes (25 by 89 mm) (87). Samples were centrifuged for 2.5 h at 50,000 rpm (50.2 Ti rotor) and 4°C. Subsequently, the 40% iodixanol fraction containing the virus was collected and analyzed by Western blotting and a capsid enzyme-linked immunosorbent assay (ELISA). Virus preparations were stored in small aliquots at −80°C.

Analyses of viral protein expression. Identical portions of harvested cells were processed for Western blot analysis. Monoclonal antibodies 303.9 and B1, specific for the Rep and VP proteins, respectively, were used as described by Wistuba et al. (76).

Quantitation of AAV2 capsids. Capsid titers were determined by an ELISA as described by Grimm et al. (24) with precoated plates supplied by Progen GmbH, Heidelberg, Germany.

Quantitation of packaged DNA. Virus supernatants (10 μl) were incubated with micrococcal nuclease (300 U/ml; Roche Diagnostics, Mannheim, Germany) in the presence of 1 mM $CaCl_2$ (pH 8) for 2 h at 37°C to digest nonpackaged DNAs. Capsid proteins were digested with proteinase K (320 μg/ml; Roche Diagnostics) at 37°C for 3 h. The samples were extracted with phenol-chloroform and concentrated by ethanol precipitation. DNA samples were diluted in 50 mM NaOH and spotted onto GeneScreen Plus nylon membranes by using a vacuum blotter (Life Technologies, Karlsruhe, Germany). ^{32}P-labeled, randomly primed probes were generated from a *rep* fragment (XhoI-BamHI) of plasmid

pBSΔTR18 (73) by using a random-primer labeling kit (Roche Diagnostics) and purified over Sephadex G50 columns. Autoradiography was carried out with Kodak Biomax MS X-ray film. The amount of DNA was determined by comparing serial dilutions of viral DNA to serial dilutions of a 4.7-kb AAV sequence with a known concentration.

Analyses of associated and packaged DNAs. In order to prevent the degradation of single-stranded genomes in virus supernatants, EDTA was used at 30 mM when cells were harvested. Immunoprecipitation of capsids was performed with protein A–Sepharose CL-4B (2 mg per sample; Amersham Pharmacia, Freiburg, Germany) in NET-N buffer (20 mM Tris, 100 mM NaCl, 1 mM EDTA, 0.5% NP-40 [pH 7.5]) containing protease inhibitor cocktail (Roche Diagnostics). Protein A-Sepharose was added to 600 μl of antibody A20 (see below) or the non-AAV-related IVA7 hybridoma supernatant, and the mixture was incubated with gentle inversion for 1 h at 4°C. The protein A-Sepharose-antibody mixture was washed twice with NET-N buffer to remove unbound antibody. Aliquots in NET-N buffer were added to virus supernatants containing equal amounts of capsids, and the mixtures were incubated overnight at 4°C with gentle inversion. The samples were washed twice with NET-N buffer and twice with TNEM buffer, resuspended in 150 μl of TNEM buffer, and either incubated or not incubated with DNase I (500 μg/ml; Roche Diagnostics) for 2 h at 37°C with gentle mixing. Subsequently, 150 μl of 2× proteinase K digestion buffer (20 mM Tris, 20 mM EDTA, 1% sodium dodecyl sulfate [pH 7.5]) and proteinase K (320 μg/ml) were added, and the mixtures were incubated for 3 h at 37°C. The DNA was extracted with phenol-chloroform and concentrated by ethanol precipitation. The DNA pellet was resuspended in water. Viral DNAs were separated on Tris-acetate-EDTA-buffered 0.8% agarose gels and then transferred to GeneScreen Plus nylon membranes in 0.4 M NaOH overnight. DNA samples were hybridized with a *rep*-specific probe as described above. The efficiency of capsid immunoprecipitation was tested by Western blot analysis with antibody B1 and portions of washed protein A-Sepharose-antibody samples that were set aside prior to proteinase K digestion.

Quantitation of infectious virus titers. HeLa cells in 100 μl of DMEM–10% FCS were plated at 10^4 cells/well on a 96-well plate 1 day prior to infection with serial dilutions of virus supernatants. At 2 h postinfection, 100 μl of DMEM containing Ad5 (MOI, 2) was added to each well. Three days later, a 0.4 volume of 1.5 M NaOH was added, and the cells were lysed by three rounds of freezing-thawing (−80 °C and 37°C). DNA was transferred to GeneScreen Plus nylon membranes by using a vacuum blotter. DNA samples were hybridized with a *rep*-specific probe as described above.

Heparin-binding assay. A column of 1 ml of heparin (Sigma) was preequilibrated with 20 ml of PBS-MK and loaded with 5 ml of 1:10-diluted virus supernatants. The column was washed twice with 5 ml of PBS-MK and eluted five times with 2 ml of PBS containing 1 M NaCl. Flowthrough, wash, and eluate fractions were analyzed by a capsid ELISA as described above.

Virus uptake. HeLa cells were grown on glass coverslips and incubated with 2.5×10^5 wild-type (wt) or mutant AAV2 particles in the absence of FCS for 30 min at 4°C. Cells were washed once with DMEM and incubated at 37°C in the presence of 10% FCS. Cells were fixed at 0, 2, and 6 h postinfection with 2% paraformaldehyde in PBS. They were washed twice with 50 mM NH_4Cl in PBS for 5 min each time, permeabilized with 0.2% Triton X-100 in PBS for 5 min, and washed again twice with PBS for 5 min each time. Cells were incubated overnight at 4°C with primary antibodies directed against capsids (A20; mouse) (76, 77) and lamin B (goat) (Santa Cruz Biotechnology, Santa Cruz, Calif.). After three washes with PBS for 10 min each time, cells were incubated with secondary antibodies labeled with Alexa 594 (Molecular Probes, Leiden, The Netherlands) (chicken anti-mouse) and Alexa 488 (Molecular Probes) (chicken anti-goat) for 1 h. Cells were washed again three times with PBS for 10 min each time. Samples were analyzed according to the uptake of capsids into cells (A20 fluorescence) by using a fluorescence microscope (Leica type DMRBE).

Determination of accessibility of N termini and stability of capsids. A total of 5×10^9 iodixanol-purified capsids in PBS-MK were exposed to various temperatures for 5 or 30 min. Samples then were incubated on ice for 5 min and transferred to Protran nitrocellulose membranes (Schleicher & Schuell, Dassel, Germany) by using a vacuum blotter. Membranes were blocked for 1 h in PBS containing 10% skim milk powder (blocking solution) and then incubated for 1 h with monoclonal antibodies A20, A1, A69, or B1 (76, 77) diluted 1:10 in blocking solution. Membranes were washed six times with PBS for 10 min each time and incubated with a peroxidase-coupled goat anti-mouse antibody (Dianova, Hamburg, Germany) for 1 h. After six washes with PBS for 10 min each time, the proteins were visualized by using an enhanced chemiluminescence detection kit (Amersham, Braunschweig, Germany).

Continuous sucrose gradient. A total of 3×10^{11} purified capsids in PBS-MK were exposed to various temperatures for 30 min. Samples were incubated on ice for 5 min and loaded onto an 11-ml 10 to 30% sucrose gradient (sucrose in PBS-MK–10 mM EDTA–protease inhibitor cocktail) in Beckman tubes (14 by 89 mm). After centrifugation at 160,000 × *g* for 2 h at 4°C (SW41 rotor; Beckman), 500-μl fractions were collected. Fractions (100 μl) were transferred to nitrocellulose membranes by using a vacuum blotter. Membranes were processed as described for the determination of accessibility of N termini and stability of capsids. For analysis of viral DNA, immunoprecipitation was performed with 150 μl of each fraction and protein A-Sepharose-bound antibody A20 before extraction of the DNA as described for the analysis of associated and packaged DNAs. DNA samples were resuspended in 50 mM NaOH and spotted onto nylon membranes by using a vacuum blotter. DNA samples were hybridized with a *rep*-specific probe as described above.

Trypsin digestion. A total of 5×10^9 iodixanol-purified capsids in 200 mM Tris-HCl–150 mM NaCl (pH 7.5) were exposed to various temperatures for 5 min. Samples were incubated on ice for 5 min, and trypsin (1 ng/μl; Roche Diagnostics) was added. The mixture was incubated at 37°C for 5, 10, or 30 min, mixed with an equal volume of 2× protein sample buffer (76) boiled immediately, and analyzed by Western blotting. Monoclonal antibodies B1, A1, and A69 were used as described above.

Cloning, expression, and purification of $Vp1His_6$ protein. The AAV2 VP1 N-terminal domain (amino acids 1 to 202) was cloned into bacterial expression vector pQcHis6 (Qiagen, Hilden, Germany). The VP1 N terminus was amplified by PCR with plasmid pTAV2.0 as a template and primers containing the EcoRI and HindIII restriction sites. The PCR product was cloned into EcoRI-HindIII of pQcHis6, and correct clones were identified by sequencing. *Escherichia coli* Rosetta (Novagen, Bad Soden, Germany) was transformed to express the VP1 N-terminal domain with a carboxy-terminal His_6 tag. $Vp1His_6$ protein was purified under native conditions on a TALON column (BD Biosciences, Heidelberg, Germany) and then dialyzed against 50 mM Tris-HCl (pH 8.0)–200 mM NaCl.

PLA2 assay. Totals of 1.5 μg of $Vp1His_6$ protein and 1.3×10^{11} wt AAV2 (or 7×10^{10} wt and mutant) virions (incubated for 5 min at various temperatures) were incubated with [1-^{14}C]oleate-labeled *E. coli* membranes as a substrate (7). Assays were performed with 100 mM Tris-HCl (pH 8.0)–10 mM $CaCl_2$–0.1% fatty acid-free bovine serum albumin (Sigma) and [1-^{14}C]oleate-labeled *E. coli* membranes (10,000 cpm). Reaction mixtures were incubated for 60 min at 37°C. Membranes were centrifuged for 3 min at 12,000 × *g*, and [1-^{14}C]oleate released into supernatants was measured by using a β-counter.

Graphics. Images were made by using Rasmol software (version 2.7.2.1.1) (55). The structure of AAV2 was obtained from the Brookhaven Protein Data Bank (entry 1LP3) (84).

Statistical analysis. Data were analyzed by an unpaired two-tailed Student *t* test and are shown as means ± standard deviations. Data were considered significant at a *P* value of less than 0.05.

RESULTS

Structures of narrow pores at the fivefold symmetry axes of AAV2 capsids. Besides three elongated spikes surrounding the threefold axes, 12 narrow pores at the fivefold axes are the most striking structural features of AAV2 capsids (Fig. 1A). These pores connect the outside of the capsid with the interior by cylindrical channels linked with a funnel-like structure, which builds the base of the pore inside the capsid (Fig. 1B). The cylinders protrude from the surrounding flat capsid surface by about 1.2 nm and are made up of antiparallel beta ribbons from each of the corresponding related capsid proteins. The interface of the beta ribbons with the funnel-like structure forms the narrowest part of the pore, at about 1.2 nm in diameter. At this site, the pore opens conically to about 2.2 nm toward the outside. A camera shutter-like arrangement of the five subunits is visible when the pore is viewed from the outside (Fig. 1C). This feature might indicate that the structure is able to alter the width of the pore. The beta ribbons, which encircle the channels, are made up of residues 322 to 338 of the VP sequence, and the funnel-like structure at the inner entrance consists of residues 217 to 223 (Fig. 1D). Sequence comparisons of AAV2 with the other seven AAV serotypes revealed that residues 217 to 223 are highly conserved, with the

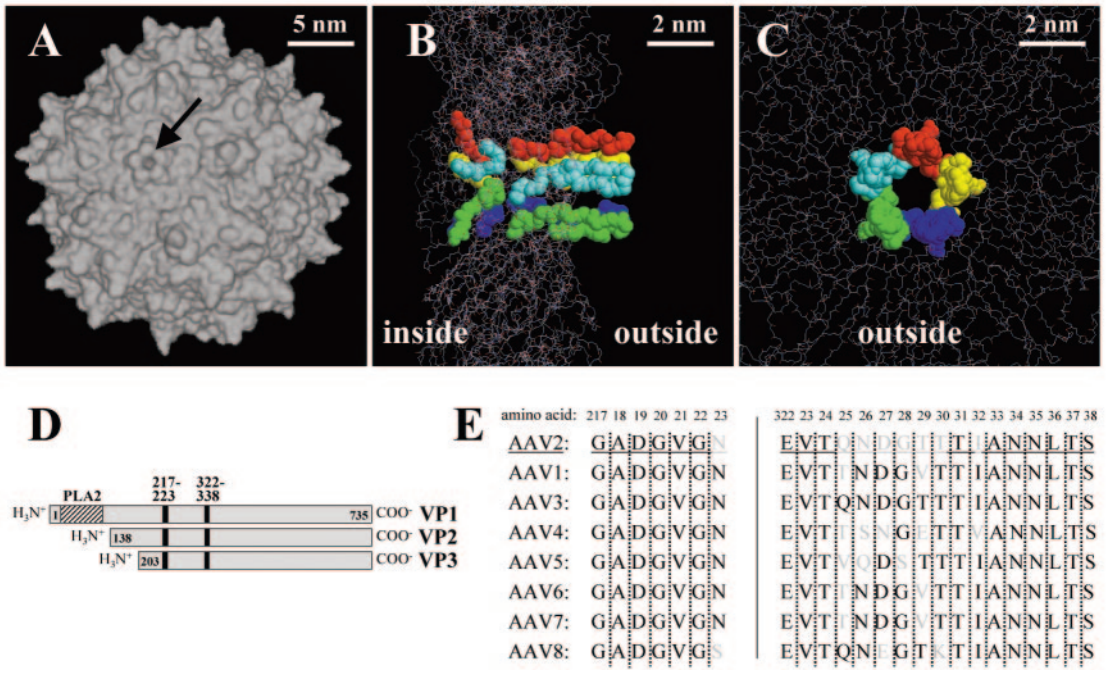

FIG. 1. Structures of pores at fivefold symmetry axes of AAV2 capsids. (A) Model of the AAV2 capsid (84); the arrow indicates the pore at a fivefold axis. (B and C) Backbone models of structures of fivefold symmetry-related VPs shown as a side view (B) and from the outside (C) of the capsid. Residues which form the pore are represented as space-filling models; different colors show that the pore is encircled by amino acids derived from each of the five subunits of the pentamer. (D) Schematic representation of the pore-forming amino acids (positions 217 to 223 and positions 322 to 338 of the VP sequence) shared by the three capsid proteins. (E) Alignment of pore-forming amino acids of eight known AAV serotypes; grey lettering indicates nonconserved amino acids.

exception of an asparagine-to-serine exchange at position 223 in AAV8 (Fig. 1E). Amino acids 322 to 338 again show a high level of conservation toward the end of the beta ribbons (residues 322 to 324 and residues 333 to 338), while residues 325 to 332 show conservative and nonconservative exchanges in the serotypes.

Site-directed mutagenesis of pore-forming amino acids. We established various mutations leading to alterations of pore-forming amino acids by using site-directed mutagenesis (Fig. 2A). Most of them were single amino acid substitutions (13 out of 16); additionally, one deletion (del219/220), one insertion (221Ins2Y), and a triple substitution (E322A/V323D/T324N) were made. Thirteen of the mutants affect conserved amino acids. Only three mutants include nonconserved residues (N223A, Q325A, and N326A). Figure 2B and C show the localization of the modified amino acids (shown in different colors) within the pore structure. In the following text these mutants are termed "pore mutants."

293T cells were transfected with plasmids harboring either an AAV2 wt genome (pTAV2.0) or genomes with mutated VP sequences. Analysis of AAV2 protein expression in extracts of transfected cells showed no significant influence of the mutations on the expression of the four Rep proteins and similar stoichiometries of the three VPs (VP1, VP2, and VP3) for the wt and the mutants (Fig. 2D). Most of the pore mutants also showed no reduction in VP expression levels compared to those in the wt. The amounts of VPs in extracts of cells transfected with mutants E322A, E322A/V323D/T324N, S338A, and V221Y were slightly decreased. Only mutant 221Ins2Y produced apparently smaller amounts of VPs.

Characterization of pore mutants. To characterize at which step of the AAV2 life cycle the pore mutants might be impaired, capsid, genome, and infectious virus titers were determined (data not shown). Most mutants showed normal capsid formation in amounts comparable to those in the wt. Only mutant 221Ins2Y was completely deficient in capsid assembly, and mutants E322A and E322A/V323D/T324N showed greatly reduced capsid assembly (5,000- and 10,000-fold). These mutants were grouped in class A (assembly mutants) (Table 1).

The packaging efficiency of the mutants was quantified by calculating the ratios of capsids to genomes and was compared to that of wt AAV2 (Fig. 3A and Table 1). No differences in genome packaging were observed for mutants N326A, L336A, T337A, and N223A. Mutants T324A, Q325A, and N335A showed a moderate reduction in packaging of approximately twofold, which was considered to be within the error range, and are therefore not classified as packaging mutants (Table 1). For mutants N334A, D219A, del219/220, V221C, and V221Y, packaging was reduced about three- to fivefold. Packaging was reduced about ninefold for mutant S338A; this reduction was comparable to the reduction seen for a small Rep-deficient construct (pTAV2.1) (Fig. 3A) (see also reference 36). These mutants were grouped in class P (packaging mutants) (Table 1). The packaging ratios could not be determined for mutants E322A and E322A/V323D/T324N (which also showed a strong reduction in capsid assembly), since the amounts of the genomes were below the detection limit (10^7) (Table 1).

In order to exclude the possibility that the observed reduction in packaging efficiency was due to inefficient DNA repli-

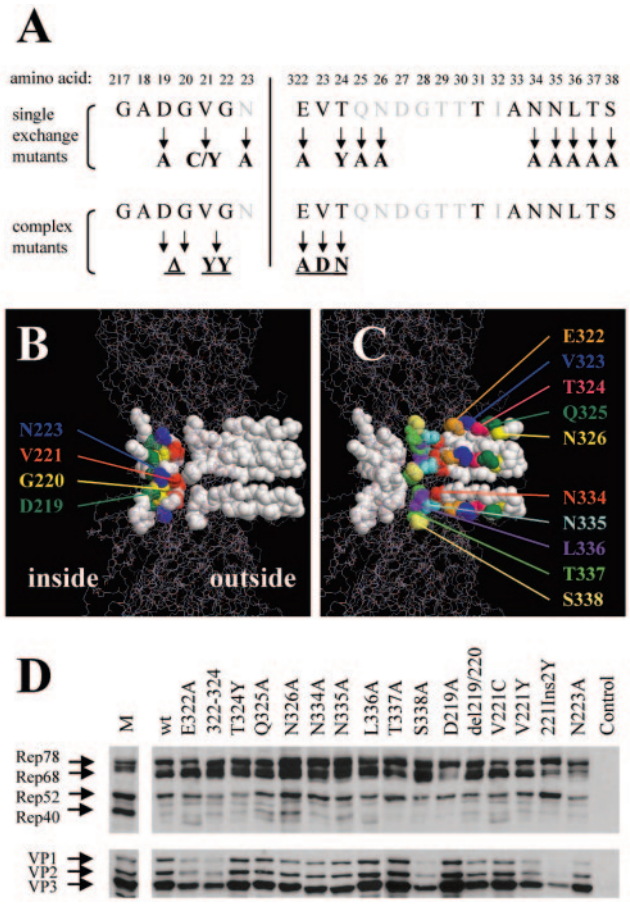

FIG. 2. Amino acids subjected to site-directed mutagenesis. (A) Residues of the AAV2 VP sequence chosen for site-directed mutagenesis (arrows denote the positions of the mutations); grey lettering indicates nonconserved amino acids. Charge-to-alanine mutations were made at positions 219, 223, 322, 325, 326, 334, 335, 336, 337, and 338; a tyrosine substitution at positions 221 and 324 and a cysteine substitution at position 221 were introduced. Additionally, a deletion of amino acids 219 and 220 (Δ), an insertion of two tyrosines after amino acid 221, and a triple substitution (amino acids 322, 323, and 324) were generated. (B and C) Localization of established mutations within pore structures at amino acids 217 and 223 (B) and amino acids 322 to 338 (C); a backbone model of a pentamer is shown as a side view. Amino acids which form the pore are represented as space-filling models; residues subjected to site-directed mutagenesis are shown in different colors. (D) Western blot analysis of 293T cells transfected with AAV2 wt or mutated genomic plasmids or Bluescript II (control) and subsequently superinfected with Ad5 (MOI, 2). AAV2 proteins were detected with monoclonal anti-Rep (303.9) or anti-VP (B1) antibodies. An extract from Ad5- and AAV2-coinfected HeLa cells was used as a marker (M).

cation, Hirt extracts were prepared (32) from 293T cells after transfection with wt or mutant AAV2 genomic plasmids and superinfection with Ad5. Southern blot analysis of DpnI-digested viral DNAs showed no differences in viral replication between the wt and the mutants (data not shown). Figure 3B shows Southern blot analysis of viral DNA after immunoprecipitation of wt or mutant virions, which revealed a three- to ninefold reduction in the amounts of packaged genomes (Table 1). Prior to genome isolation, the samples were either treated or not treated with DNase I. For wt AAV2, dominant 4.7-kb ssDNA bands were visible in both DNase I-treated and untreated samples, and no nuclease-sensitive DNA could be detected; these results indicated that full-length genomes had been efficiently packaged. The pore mutants also showed comparable amounts of DNA in both DNase I-treated and untreated samples, but the amounts of encapsidated DNA were smaller than those seen for wt AAV2. In contrast, for a small Rep-deficient construct, AAV2 DNA was incompletely packaged, and full-length capsid-associated DNA was nuclease sensitive (Fig. 3B) (see also reference 36). Immunoprecipitations with a non-AAV-related monoclonal antibody (Fig. 3B, control [C]) controlled the specificity of the precipitations. Western blot analysis of A20-precipitated samples verified that equal amounts of capsids were analyzed. These results clearly demonstrate that mutants N334A, V221C, V221Y, S338A, D219A, and del219/220 in fact exhibited a packaging defect which led to reduced but not partial DNA encapsidation.

Infectious virus titers, determined as replicative units in the presence of Ad5, were reduced for many of the mutants compared to wt AAV2 (data not shown). The ratios of genomes to infectious units were calculated for the mutants and were compared to the ratio for the wt to quantify the effects on infectivity and to correct for the observed reduction in the packaging of some mutants (Fig. 4 and Table 1). This analysis demonstrated that mutants S338A, del219/220, V221C, and V221Y were affected in both packaging and infectivity (class P + I) (Table 1). On the other hand, mutants T324Y, N335A, L336A, and T337A were affected only in their infectivity, a finding clearly demonstrating that some pore mutants are impaired in only one of the two different processes. These mutants were grouped in class I (infectivity mutants) (Table 1). Some mutants did not exhibit detectable differences from the wt (Q325A, N326A, and N223A). The mutations in these mutants affect only amino acids which are not conserved in AAV serotypes; these mutants were grouped in class N (not affected mutants) (Table 1).

Receptor binding and virus uptake. During virus infection, binding to the cell receptor and cell entry are the first steps to be analyzed. As shown in Table 1, there were no significant differences between any of the pore mutants and wt AAV2 with respect to heparin binding. This binding indicates that the mutants were able to bind to heparan sulfate proteoglycan on 293T cells, used for the infectivity assays, and that they were most likely internalized. This assumption was tested for the mutants which showed the most severely reduced infectivity by indirect immunofluorescence (data not shown). The virus uptake of these mutants was indistinguishable from that of wt AAV2 (Table 1). wt as well as mutant virions accumulated perinuclearly 4 h after infection. Taken together, these observations prove that the reduction in infectivity is not a result of decreased receptor binding or cellular uptake of mutant virions.

PLA2 activity of wt AAV2 virions. Among the postentry events in AAV2 infection characterized so far, the activity of a PLA2 domain located on the unique N terminus of VP1 plays an important role in the establishment of a productive infection (22). Native AAV2 capsids showed no PLA2 activity (Fig. 5). This finding is in agreement with our hypothesis that the N terminus of VP1 is located at the inner surface of intact AAV2 capsids (37). Previous studies demonstrated that VP1 N termini of autonomous parvoviruses, such as MVM and CPV,

TABLE 1. Characterization of AAV2 pore mutants

Mutation(s)	Packaging reduction with respect to wt[a,b]	Infectivity reduction with respect to wt[a,c]	Heparin binding[d]	Virus uptake[e]	Class[f]
E322A	UD	UD	+	ND	A
E322A/V323D/T324N	UD	UD	+	ND	A
T324Y	2.0 ± 0.8	32 ± 8	+	ND	I
Q325A	1.7 ± 0.5	4.5 ± 0.5[g]	+	ND	N
N326A	0.7 ± 0.1	1.2 ± 0.1	+	ND	N
N334A	3.8 ± 1.5[g]	1.1 ± 0.1	+	ND	P
N335A	2.0 ± 0.5[g]	2.1E4 ± 1.3E4[g]	+	+	I
L336A	1.2 ± 0.1	1.8E2 ± 0.5E2[g]	+	ND	I
T337A	1.1 ± 0.1	37 ± 12[g]	+	ND	I
S338A	8.9 ± 2.1[g]	1.1E3 ± 0.7E3[g]	+	+	P+I
D219A	4.9 ± 1.2[g]	1.1 ± 0.1	+	ND	P
del219/220	4.6 ± 1.5[g]	61 ± 14[g]	+	+	P+I
V221C	3.2 ± 0.3[g]	2.8E2 ± 0.4E2[g]	+	ND	P+I
V221Y	3.4 ± 0.7[g]	1.7E3 ± 0.8E3[g]	+	+	P+I
221Ins2Y	UD	UD	UD	ND	A
N223A	0.5 ± 0.1[g]	1.3 ± 0.1[g]	+	ND	N

[a] Values are means plus or minus standard deviations from at least four independent experiments; UD, undetectable.
[b] Packaging was measured as the ratio of capsids to viral genomes and compared to the ratio for wt AAV2. The number of assembled capsids was determined by a capsid ELISA (24); packaged DNA was quantified by a dot blot assay.
[c] Infectivity was expressed as the ratio of genomes to infectious units and compared to the ratio for wt AAV2. Packaged DNA was measured by a dot blot assay; infectious AAV2 particles were quantified by a dot blot replication assay.
[d] Heparin binding was measured as the percentage of viral particles which were applied to a heparin-agarose column and which were recovered by high-salt elution, as determined by a capsid ELISA; +, more than 90% binding.
[e] Virus uptake (+) into cells was analyzed by indirect immunofluorescence microscopy. ND, not determined.
[f] Mutants were classified according to their defects: A, assembly (more than a 10-fold reduction compared to that in the wt); I, infectivity (more than a 10-fold reduction compared to that in the wt); P, packaging (more than a 2-fold reduction compared to that in the wt); N, not affected.
[g] In a comparison with the wt, the P value was <0.05.

become accessible on intact virions after treatment with heat or urea (15, 69). In order to investigate whether heat treatment also leads to the activation of PLA2 activity of AAV2 virions, the virions were incubated for 5 min at various temperatures before PLA2 activity was measured (Fig. 5). Treatment of AAV2 virions at 60°C revealed some PLA2 activity, suggesting that at least part of the VP1 N termini became accessible either by exposure at the capsid surface or by partial dissociation of some capsids. After incubation of virions at 65°C, PLA2 activity was even increased and reached levels comparable to that of the bacterially expressed PLA2 domain. PLA2 activity was significantly reduced after treatment of particles at 75°C compared to 65°C. This effect might have been due to partial denaturation of the enzymatic domain at the higher temperature.

Exposure of VP1 N termini and stability of wt virions after heat treatment. The activation of PLA2 activity upon heat treatment correlates with the exposure of VP1 N termini. A more specific analysis of the exposure of VP1 N termini was conducted by using monoclonal antibodies which react with defined epitopes on capsids or capsid proteins (Fig. 6A). Whereas antibody A20 recognizes whole capsids but not dissociated capsid proteins (77), antibody A1 detects an epitope close to the PLA2 domain on the N terminus of VP1. Antibody A69 reacts with an epitope common to VP1 and VP2 (78). Antibody B1 recognizes amino acids 726 to 733 at the C termini of all three capsid proteins (78). After incubation of virions for 30 min at 37°C, intact capsids were detected by antibody A20 upon application to nitrocellulose under nondenaturing conditions (Fig. 6B). Only a very weak reaction with antibodies A1 and A69 could be detected, indicating that VP1 N termini on these capsids were only partially accessible to the antibodies. This reaction was strongly increased after incubation of virions at 60°C, while the reaction with the capsid-specific antibody (A20) was unchanged. Only a weak reaction with antibody B1 was detected. After incubation at 65°C, both N-terminal (A1 and A69) and C-terminal (B1) epitopes became accessible. Capsids were completely disrupted after incubation at 75°C, as indicated by the loss of the antibody A20 reaction.

In order to discriminate whether the reactions of N- and C-terminus-specific antibodies with virions treated at 60 or 65°C were due to partial dissociation of the capsids or to a conformational change, we analyzed heat-treated virus preparations on a continuous sucrose gradient (Fig. 6C). This gradient allowed us to distinguish among DNA-containing, empty, and dissociated particles sedimenting at 110S, at 60S, and below 20S, respectively. After incubation at 37°C, virions sedimented with a peak at about 110S, as detected by antibody A20. A weak signal at the same position with antibody A69 showed that in some capsids, the epitope is accessible to the antibody. The reaction with antibody A69 was strongly enhanced after treatment at 60°C, together with enhanced binding of antibody A1. These results clearly indicate a conformational change in intact capsids sedimenting at 110S and reacting with antibody A20. A second conformational change seemed to be initiated after 65°C heat treatment, as indicated by the reaction with antibody B1 and the appearance of a second peak of antibody A20-reactive particles sedimenting slightly beyond 60S. The peak was characterized by a low DNA content (Fig. 6D) and was most likely derived from the 110S fraction by the release of AAV2 genomes. This structure was not observed in some preparations after incubation at 65°C, indicating that the exact temperature at which DNA is released from capsids may depend on additional parameters of the virus preparations (e.g., salt concentration, age, and number of freezing-thawing cycles). Dissociated and aggregated material was detected by

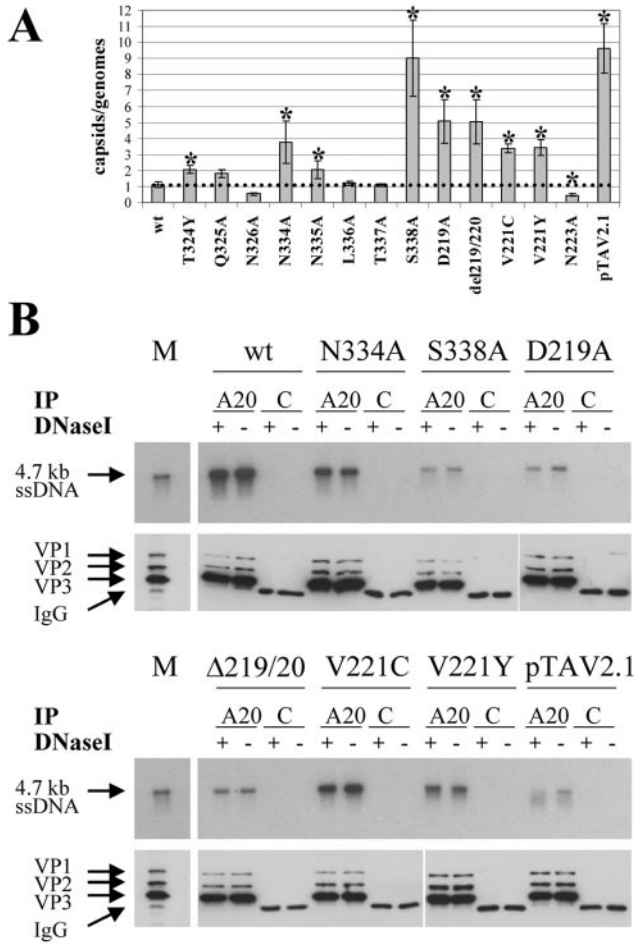

FIG. 3. Influence of mutation of pore-forming amino acids on genome packaging. (A) Virus supernatants obtained from 293T cells transfected with an AAV2 wt or mutated genomic plasmid (pTAV2.1: small Rep-deficient mutant) and superinfected with Ad5 (MOI, 2) were assayed for ELISA-based AAV2 capsid titers and dot blot-based genomic titers. Packaging was quantified as the ratio of capsids to genomes. Means ± standard deviations from at least four independent experiments are shown; an asterisk indicates a P value of <0.05 for a comparison with the wt value (indicated by the broken line). (B) Capsids were immunoprecipitated (IP) from frozen-thawed lysates obtained from 293T cells transfected with a plasmid harboring an AAV2 wt or mutated genome and superinfected with Ad5 (MOI, 2) by protein A-Sepharose-bound antibody A20. Control (C) precipitations were also performed with a non-AAV-related monoclonal antibody. Samples were digested (+) or not digested (−) with DNase I to discriminate between capsid-associated and packaged DNAs. Coprecipitated genomes were isolated and electrophoresed on neutral agarose gels. Southern blotting was performed, and genomes were detected with a *rep*-specific probe. A 4.7-kb fragment was used as a marker (top panels, M). A portion of each immunoprecipitate was tested by Western blot analysis for the level of capsid recovery; an extract from Ad5- and AAV2-coinfected HeLa cells was used as a marker (bottom panels, M).

antibodies B1 and A69 all over the gradient after treatment at 75°C. The material did not react with antibody A20. The observed low binding reactivity with antibody A1 in gradient fractions after treatment at 75°C could be explained by proteolytic degradation of the VP1 N terminus.

These results clearly show that DNA-containing AAV2 capsids undergo a conformational change when they are incubated

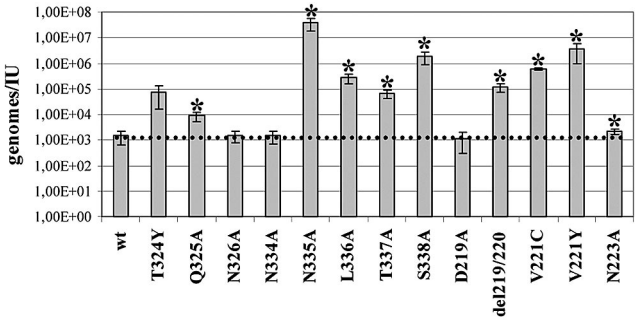

FIG. 4. Effect of mutation of pore-forming amino acids on infectivity. Virus supernatants obtained from 293T cells transfected with an AAV2 wt or mutated genomic plasmid and superinfected with Ad5 (MOI, 2) were assayed for dot blot-based genomic titers and dot blot-based infectious virus titers. Infectivity was quantified by calculating the ratios of genomes to infectious units (IU). This calculation corrects for the observed reduction in the packaging of some mutants. Means ± standard deviations from at least four independent experiments are shown; an asterisk indicates a P value of <0.05 for a comparison with the wt value (indicated by the broken line).

at 60°C, a process which leads to the exposure of VP1 N termini. Incubation at 65°C revealed a second structural rearrangement characterized by a fraction with low DNA content and sedimenting below 60S. This structural change may represent a further discrete step in AAV disassembly.

Accessibility of VP1 N termini and heat stability of pore mutants. We next examined whether mutation of pore-forming amino acids had an impact on the presentation of VP1 N termini on the capsid surface. Such a finding would implicate a role of the pores at the fivefold symmetry axes in the activation of PLA2 activity during infection. Thus, mutants which had a strong negative effect on viral infectivity were selected to analyze the possible role of the pores. First, the compositions of assembled capsids were determined by Western blot analyses of purified capsids (Fig. 7A). No major differences in the stoichiometric ratios of VP1, VP2, and VP3 in assembled capsids were observed between the mutants and the wt. The accessibility of antibody epitopes was analyzed in a native dot blot

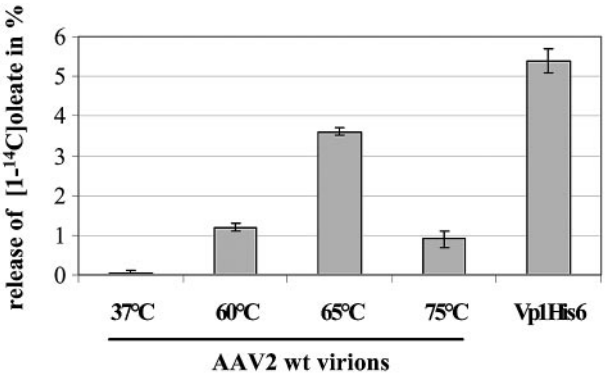

FIG. 5. PLA2 activity of heat-treated AAV2 wt virions. AAV2 virions were exposed to various temperatures for 5 min and then incubated with [1-^{14}C]oleate-labeled *E. coli* membranes. The release of [1-^{14}C]oleate into supernatants was measured. As a positive control, the assay was performed with purified Vp1His$_6$. Means ± standard deviations from at least three independent experiments are shown.

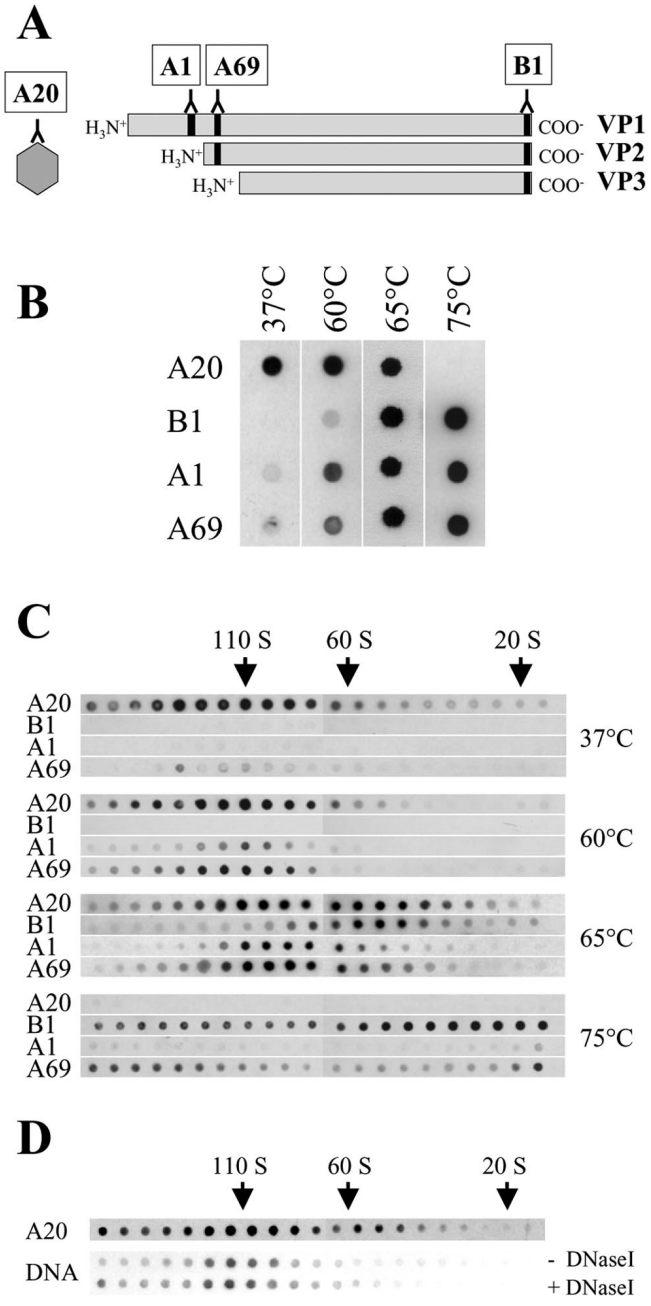

FIG. 6. Exposure of VP1 N termini after heat treatment of AAV2 wt virions. (A) Localization of epitopes recognized by antibodies A20, A1, A69, and B1 in the native dot blot assay. (B) Native dot blot assay. AAV2 wt virions were exposed to various temperatures for 30 min and then reacted under nondenaturing conditions with antibodies A20, B1, A1, and A69. (C) AAV2 wt virions were incubated at various temperatures for 30 min and then loaded onto a continuous sucrose gradient (10 to 30% sucrose). Aliquots of each fraction were subjected to the native dot blot assay and probed with antibodies A20, B1, A1, and A69. (D) AAV2 wt virions were incubated at 65°C for 30 min and then loaded onto a continuous sucrose gradient (10 to 30% sucrose). Aliquots of each fraction were subjected to the native dot blot assay and detected with antibody A20. Another aliquot of each fraction was immunoprecipitated with antibody A20 and incubated with or without DNase I, and coprecipitated genomes were detected with a *rep*-specific probe. The 110S, 60S, and 20S positions were determined by using DNA-containing AAV2 particles, empty AAV2 particles, and thyroglobulin.

assay. No differences were observed between the wt and the mutants after incubation of virions for 5 or 30 min at 37 and 75°C (Fig. 7B). Capsids remained intact (reaction with antibody A20) after treatment at 37°C, and only very weak reactions with antibodies A1 and A69 could be detected. All capsids were disrupted after incubation at 75°C, as indicated by the loss of a reaction with antibody A20. Striking differences were observed between the wt and the pore mutants after heat treatment for 5 min at 60 and 65°C. Typically, wt capsids remained intact (reaction with antibody A20) and exposed their VP1 N termini (reactions with antibodies A1 and A69). However, most mutants (five out of seven) showed reduced or no presentation of VP1 N termini, as indicated by reactions with antibodies A1 and A69 (mutants N335A, V221C, L336A, del219/220, and V221Y). In addition, some mutants showed increased antibody B1 binding, indicating accessibility of the C terminus, and decreased stability, indicated by a loss of detection by antibody A20 at 65°C (mutants L336A, del219/220, V221Y, S338A, and T324Y). These effects were enhanced after 30 min of incubation. The accessibility of the N termini of those mutants was most likely due to partial or complete dissociation of the capsids, as indicated by the loss of a reaction with antibody A20 after incubation at 65°C for 30 min. Controls for pore mutants with a phenotype only in packaging or without a phenotype showed exposure of VP1 N termini and stability of the capsids at 60 and 65°C comparable to those of wt AAV2. However, reactions with antibody B1 were enhanced after prolonged incubation times (data not shown).

Trypsin digestion of heat-treated capsids. Proof of the interpretation that the exposure of VP1 N termini is blocked in certain pore mutants was provided by assessing the accessibility of AAV2 VP1 N termini to trypsin digestion. Purified wt or mutant capsids were exposed for 5 min to various temperatures and then digested with trypsin for 5, 10, or 30 min (Fig. 8). wt virions preincubated at 37°C showed no cleavage. However, a cleavage product migrating between VP2 and VP3 was obtained after heat treatment at 60°C (Fig. 8A). The amount of this cleavage product increased after incubation at 65°C, while the amount of VP1 decreased. The effect was enhanced after incubation at 70°C and was accompanied by reduced amounts of all three VPs, indicating that the capsids were partially disrupted and therefore sensitive to trypsin digestion. Reaction of the trypsin cleavage product after incubation of virions at 60 or 65°C with N-terminus-specific antibodies clearly showed that it still could be detected by antibody A69 but not by antibody A1 (Fig. 8B). These data indicate that the cleavage occurred between the epitopes recognized by antibody A1 (amino acids 123 to 131) and antibody A69 (amino acids 171 to 182) (78). We therefore concluded that the exposed N terminus of VP1 is removed.

Trypsin digestion of mutant capsids clearly indicated a deficiency in the exposure of VP1 N termini of mutants N335A, V221C, L336A, del219/220, and V221Y after pretreatment at 60 or 65°C (Fig. 8C). Mutants S338A and T324Y had accessible N termini after pretreatment at 60 and 65°C, respectively. However, this feature was already accompanied by the disintegration of capsids, as shown in the dot blot assay (Fig. 7B). The capsids of all mutants, like the wt capsids, were sensitive to trypsin digestion after incubation at 70°C, a finding which was most likely due to impaired capsid integrity.

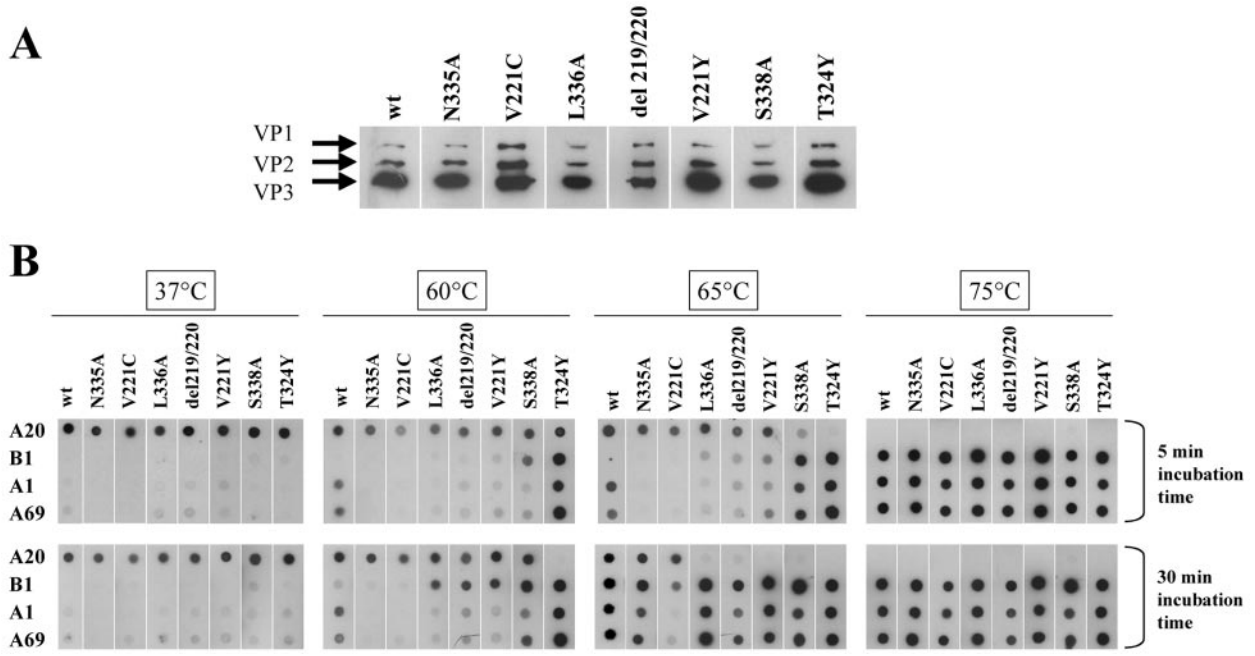

FIG. 7. Influence of mutation of pore-forming amino acids on the accessibility of VP1 N termini after heat treatment. (A) Western blot analysis of AAV2 wt or mutant virus preparations with anti-VP monoclonal antibody B1. (B) AAV2 wt or mutant virions were incubated at various temperatures for 5 or 30 min, applied to nitrocellulose membranes, and then reacted under nondenaturing conditions with antibodies A20, B1, A1, and A69.

These results confirm the observations made for the accessibility of antibody epitopes located on the VP1 and VP1-VP2 N termini, described above. They strongly suggest that N termini of VP1 harboring the PLA2 domain can be exposed on the capsid surface through the pores at the fivefold symmetry axes. The reduced infectivity of the pore mutants could be explained by the deficiency of these mutants in presenting the PLA2 domain through the pores on intact capsids during AAV2 infection.

PLA2 activity of pore mutants. To verify that the mutation of pore-forming amino acids affected the activation of PLA2 activity, two mutants were selected for the PLA2 assay (Fig. 9). Mutant V221C, which was restricted in presenting VP1 N termini at 60 and 65°C, showed almost no PLA2 activity after pretreatment of the virions at 60°C. Incubation at 65°C revealed very weak activity, which was clearly lower than that of wt AAV2 virions. Higher PLA2 activity was measured for mutant T324Y after incubation at 60 and 65°C than for the wt. The increase was most likely due to the accessibility of VP1 N termini on disrupted capsids at these temperatures, as shown in the dot blot assay (Fig. 7B). These results clearly show that the activation of PLA2 activity on intact capsids is affected by the mutation of pore-forming amino acids. They further suggest that the activation of PLA2 activity in unstable capsids is not sufficient for successful infection.

DISCUSSION

The capsid structure of parvoviruses shows open pores of unknown function at each of the fivefold symmetry axes. They are large enough to allow passage of macromolecules such as nucleic acids or protein domains in an extended conformation. We generated various mutations of amino acids involved in the formation of these pores and analyzed their influence on capsid assembly, genome packaging, and infectivity. Mutations in residues which are conserved among AAV serotypes resulted in phenotypes in one or two of the viral activities analyzed, whereas mutations in nonconserved amino acids resulted in no detectable phenotype.

Assembly. So far, the molecular steps in AAV2 capsid assembly are not well established. Mutational analysis of AAV2 capsid proteins revealed that mutations within the beta-barrel structure and at the very N or C terminus of VP3 impaired assembly (53, 72, 80). It was shown for MVM that a few residues involved in intertrimer interactions have a crucial role in capsid assembly and stability (51). In cells expressing CPV proteins, small amounts of trimers could be detected (85). There is some evidence for AAV2 that trimers or pentamers may function as intermediates in the assembly process (76). Most of the generated pore mutants showed normal capsid formation (Table 1). Insertion of two tyrosine residues after position 221 completely abolished capsid assembly, suggesting that the insertion of two bulky residues may impair interactions between related capsid proteins. In two other mutants (E322A and E322A/V323D/T324N), also impaired in capsid formation, affected amino acid residues were located at the boundary between the core tertiary structure of the VPs and the pore-forming beta ribbons at the fivefold axes. Assuming that pentamer formation is an essential step in AAV2 assembly, it is conceivable that the side chains of these amino acids influence the geometry of subunit interactions and thereby impair capsid assembly. In support of this notion, it was shown that the exchange of a leucine within the fivefold pore structure of MVM capsids interferes with capsid formation (20).

Packaging. Viruses package their genomes into a protein shell either by association of structural proteins with the viral DNA or by translocation of viral genomes into preformed

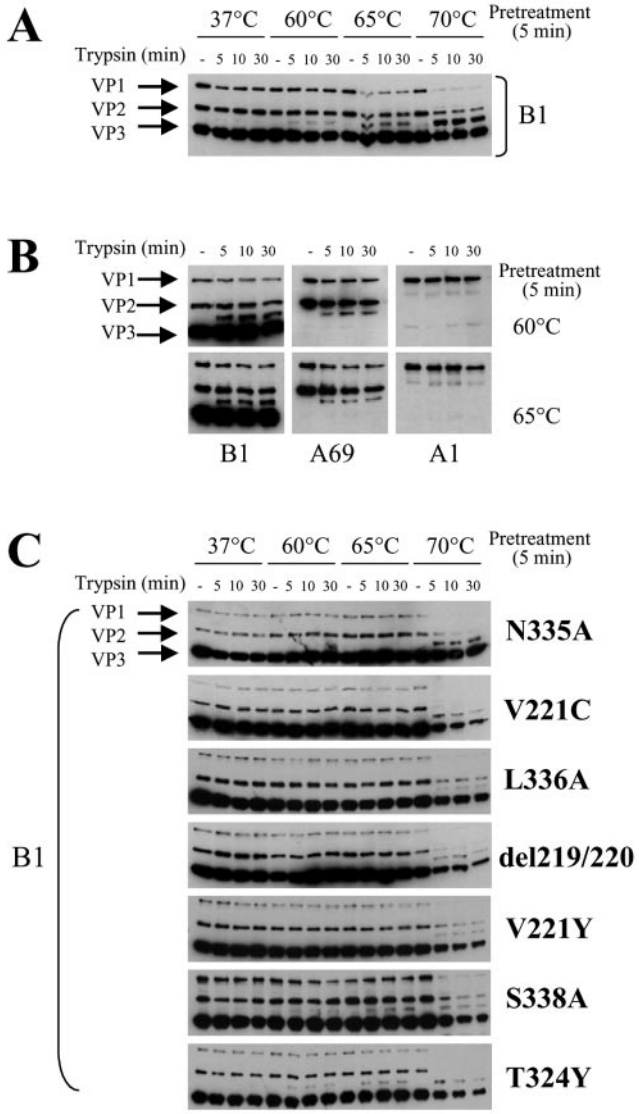

FIG. 8. Accessibility of VP1 N termini to trypsin digestion. (A and B) AAV2 wt virions were incubated at various temperatures for 5 min, treated with trypsin for 5, 10, or 30 min, and then analyzed by Western blotting. VPs were detected with antibody B1 (A) or antibodies B1, A69, and A1 (B). (C) Mutant virions were incubated at various temperatures, treated with trypsin for 5, 10, or 30 min, and then analyzed by Western blotting. VPs were detected with antibody B1.

capsids (25, 29, 44, 48, 68). Insertion of viral genomes into preassembled procapsid through a portal protein complex to which packaging enzymes bind in complex with the concatemeric DNA has been shown for viruses with double-stranded linear genomes, such as bacteriophages and herpesviruses. DNA is translocated into the capsid in an ATP-dependent fashion (12, 21). The single-stranded genome of AAV2 is thought to be packaged into procapsids as well (36, 46). The AAV2 large and small Rep proteins display a spectrum of activities very similar to those of the bacteriophage packaging complex, namely, sequence-specific DNA binding, ATPase, endonuclease, and helicase activities (45). In addition, the Rep proteins were found to form complexes with AAV2 capsids (19), and the helicase activity of the small Rep proteins present in encapsidation complexes is proposed to drive ssDNA translocation into procapsids (13, 36). The AAV2 Rep40 helicase is a member of the SF3 helicase family and is structurally related to the AAA^+ family of motor proteins (33). Structural features directly imply the requirement of Rep40 oligomerization for ATP hydrolysis and helicase activity. A hexameric ring-like model similar to that for other SF3 helicase could be predicted for the Rep40 helicase and might indicate a possible portal-motor-type function operating at a portal vertex-like structure to translocate the viral genome into the capsid.

In this study, we showed that mutation of amino acids surrounding the fivefold pore of AAV2 capsids impaired genome packaging (Fig. 3 and Table 1). These data indicated that the pores may form the portal for DNA encapsidation. Mutations which affect packaging concern residues which are located directly at or close to the tightest part of the pore (Fig. 2). The fact that no partial packaging could be observed argues in favor of overall reduced translocation due to hindered passage through the pores rather than a block at a certain step in the translocation reaction. It would be of interest to determine whether blocking of the channel by bulky residues could prevent packaging more efficiently. The insertion of two tyrosines after amino acid 221 was performed with the intention to plug the pores, but unfortunately this mutant did not assemble. However, Farr and Tattersall (20) observed an almost complete interruption of packaging after a leucine-to-tryptophan exchange within the fivefold pore structure of MVM capsids. This observation strongly suggested that this finding was due to impermeable pores at the fivefold symmetry axes. Also, a reduced docking reaction could account for the decreased amount of packaged DNA. Since the mutated amino acids are not accessible at the outside of the capsid, they would have to have a conformational effect on the docking of the packaging machinery to the capsid. However, it is conceivable that packaging efficiency declines if the geometry of the interaction between Rep proteins and capsids is impaired. Further investigations are required to elucidate the precise mechanism(s) which leads to reduced packaging after mutation of different pore-forming amino acids.

Infectivity. Virion structures have to be metastable to permit rearrangements and conformational changes during cell entry,

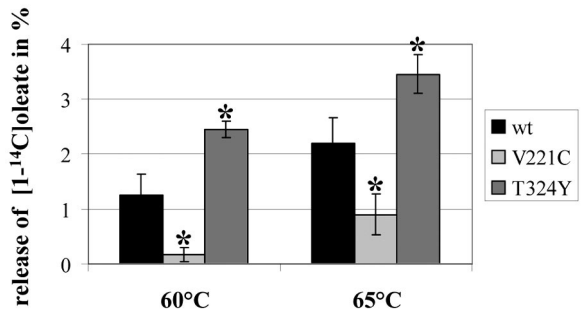

FIG. 9. Effect of mutation of pore-forming amino acids on PLA2 activity. AAV2 wt and mutant virions were exposed to 60 and 65°C for 5 min and then incubated with [1-^{14}C]oleate-labeled *E. coli* membranes. The release of [1-^{14}C]oleate into supernatants was measured. Means ± standard deviations from at least three independent experiments are shown; an asterisk indicates a P value of <0.05 for a comparison with the wt value.

finally resulting in successful delivery of the viral genome into the host cell (60). Such conformational transitions can be induced experimentally by exposure of virions to an external energy source, such as heat, or to denaturing agents (16, 43). In this study, we showed that AAV2 wt virions undergo specific conformational changes when incubated at 60 or 65°C. These transitions led to externalization of the unique N-terminal region of VP1 on intact capsids and the release of the AAV2 genome (Fig. 6). The VP1 N termini harbor a PLA2 domain and possibly other functional elements required for efficient infection. We further showed that PLA2 activity could be triggered by heating AAV2 virions at 60 or 65°C (Fig. 5). Similar observations were made for autonomous parvoviruses, such as CPV, MVM, and porcine parvovirus (11, 15, 62, 69, 86). These results suggest that the exposure of VP1 N termini on parvovirus virions is a prerequisite for the activation of PLA2 activity of virions. In this study, we were able to link reduced infectivity of pore mutants to an impaired presentation of VP1 N termini, which resulted in inefficient activation of PLA2 activity on intact AAV2 capsids by heat treatment. Pore mutants which showed accessible N termini and PLA2 activity after heat treatment also showed reduced capsid stability (Fig. 7 and 8). The reduced infectivity of these less stable mutants suggests that the activation of PLA2 activity is required while the AAV2 genome is still protected inside the capsid. Impaired presentation of VP1 N termini may also affect the nuclear import of incoming virions. A consensus nuclear localization sequence has been mapped for MVM and CPV at the VP1 N-terminal region. The nuclear localization sequence has been suggested to mediate the nuclear transport of capsids after they enter the cytoplasm (41, 69). Although these regions are not conserved in AAV2, related sequence motifs in the AAV2 VP1 and VP2 N termini may exhibit similar functions.

Combined with our structural analysis of the localization of VP1 and VP2 N termini within the capsid before and after heat treatment (S. Kronenberg, B. Böttcher, W. von der Lieth, S. Bleker, and J. A. Kleinschmidt, submitted for publication), our data strongly suggest that the VP1 N termini become exposed through the pores at the fivefold symmetry axes as part of the AAV2 infection process. Several observations with autonomous parvoviruses also support this interpretation. It has been shown for MVM that mutants with substitutions of residues close to the fivefold pores were not able to undergo the conformational transition induced by mild heating, which normally leeds to exposure of VP2 N termini on wt VP2 capsids only (51). The fivefold pores are partially filled in almost all of the resolved structures of parvoviruses (2, 3, 40, 83). Molecular modeling suggests that part of the AAV2 VP1 N terminus also can be accommodated in fivefold pores (Kronenberg et al., submitted). Furthermore, insertions of foreign epitopes at the N terminus of VP1 or VP2 have been found to be presented on the surface of mutant virions, as indicated by their accessibility to antibodies (57, 72, 80). These data suggest that unrelated protein domains also are able to unfold and travel through pores. Alternatively, they could become exposed during the assembly process.

As described above, some mutations of conserved residues surrounding the fivefold pores reduce packaging and infectvity, whereas other mutants are only affected in one of these two processes. Such functional overlapping between residues and substructures might be due to an adaptive evolution toward relatively simple capsid structures combining several functions. The pores at the fivefold axes of AAV2 virions may provide a way in which to expose VP1 N termini during infection for activation of PLA2 activity and maybe other domains. At least one axis is presumably occupied by DNA and may represent the portal where DNA encapsidation occurs.

Comparison to other viruses. Some other viruses with icosahedral capsids make use of pores at the fivefold axes of symmetry to release nucleic acids or functional protein domains. For picornaviruses, it is supposed that after binding to the cellular receptors, an iris-type movement of major capsid protein VP1 occurs to open up a channel at the fivefold axes, which leads to exposure of the N terminus of VP1. Minor capsid protein VP4, which clusters on the inner surface under the fivefold channel, is assumed to be externalized through this channel, and the viral RNA genome is subsequently released into the cytoplasm (8, 30, 31). Reoviruses potentially release newly synthesized mRNAs transcribed within the intact capsid through pores at the fivefold symmetry axes (18, 52, 81).

The mutational analysis of pore-forming amino acids of AAV2 capsids supports further the general concept that viral capsids contain pores through which macromolecules such as protein domains or nucleic acids can be translocated. The mechanisms by which these translocation processes occur are still largely unknown. It is one of the major goals to establish the physiological conditions under which the activation of pores for DNA translocation or passage of protein domains occurs.

ACKNOWLEDGMENTS

We thank Celina Cziepluch and Ute Koch for critical reading of the manuscript and Marietta Kaszkin for providing the [1-^{14}C]oleate-labeled *E. coli* membranes and introducing us to the PLA2 assay.

REFERENCES

1. **Agbandje, M., R. McKenna, M. G. Rossmann, M. L. Strassheim, and C. R. Parrish.** 1993. Structure determination of feline panleukopenia virus empty particles. Proteins **16:**155–171.
2. **Agbandje, M., S. Kajigaya, R. McKenna, N. S. Young, and M. G. Rossmann.** 1994. The structure of human parvovirus B19 at 8 A resolution. Virology **203:** 106–115.
3. **Agbandje-McKenna, M., A. L. Llamas-Saiz, F. Wang, P. Tattersall, and M. G. Rossmann.** 1998. Functional implications of the structure of the murine parvovirus, minute virus of mice. Structure **6:**1369–1381.
4. **Atchison, R. W., B. C. Casto, and W. M. Hammon.** 1965. Adeno-associated defective virus particles. Science *1***49:**754–756.
5. **Bartlett, J. S., R. Wilcher, and R. J. Samulski.** 2000. Infectious entry pathway of adeno-associated virus and adeno-associated virus vectors. J. Virol. **74:** 2777–2785.
6. **Becerra, S. P., F. Koczot, P. Fabisch, and J. A. Rose.** 1988. Synthesis of adeno-associated virus structural proteins requires both alternative mRNA splicing and alternative initiations from a single transcript. J. Virol. **62:** 2745–2754.
7. **Beck, S., G. Lambeau, K. Scholz-Pedretti, M. H. Gelb, M. J. Janssen, S. H. Edwards, D. C. Wilton, J. Pfeilschifter, and M. Kaszkin.** 2003. Potentiation of tumor necrosis factor alpha-induced secreted phospholipase A2(sPLA2)-IIA expression in mesangial cells by an autocrine loop involving sPLA2 and peroxisome proliferator-activated receptor alpha activation. J. Biol. Chem. **278:**29799–29812.
8. **Belnap, D. M., D. J. Filman, B. L. Trus, N. Cheng, F. P. Booy, J. F. Conway, S. Curry, C. N. Hiremath, S. K. Tsang, A. C. Steven, and J. M. Hogle.** 2000. Molecular tectonic model of virus structural transitions: the putative cell entry states of poliovirus. J. Virol. **74:**1342–1354.
9. **Buller, R. M., J. E. Janik, E. D. Sebring, and J. A. Rose.** 1981. Herpes simplex virus types 1 and 2 completely help adenovirus-associated virus replication. J. Virol. **40:**241–247.
10. **Canaan, S., Z. Zadori, F. Ghomashchi, J. Bollinger, M. Sadilek, M. E. Moreau, P. Tijssen, and M. H. Gelb.** 2004. Interfacial enzymology of parvovirus phospholipases A2. J. Biol. Chem. **279:**14502–14508.

11. **Carreira, A., M. Menendez, J. Reguera, J. M. Almendral, and M. G. Mateu.** 2004. In vitro disassembly of a parvovirus capsid and effect on capsid stability of heterologous peptide insertions in surface loops. J. Biol. Chem. **279:** 6517–6525.
12. **Catalano, C. E.** 2000. The terminase enzyme from bacteriophage lambda: a DNA-packaging machine. Cell. Mol. Life Sci. **57:**128–148.
13. **Chejanovsky, N., and B. J. Carter.** 1989. Mutagenesis of an AUG codon in the adeno-associated virus rep gene: effects on viral DNA replication. Virology **173:**120–128.
14. **Clinton, G. M., and M. Hayashi.** 1976. The parvovirus MVM: a comparison of heavy and light particle infectivity and their density conversion in vitro. Virology **74:**57–63.
15. **Cotmore, S. F., A. M. D'Abramo, Jr., C. M. Ticknor, and P. Tattersall.** 1999. Controlled conformational transitions in the MVM virion expose the VP1 N-terminus and viral genome without particle disassembly. Virology **254:** 169–181.
16. **Curry, S., M. Chow, and J. M. Hogle.** 1996. The poliovirus 135S particle is infectious. J. Virol. **70:**7125–7131.
17. **Dorsch, S., G. Liebisch, B. Kaufmann, P. von Landenberg, J. H. Hoffmann, W. Drobnik, and S. Modrow.** 2002. The VP1 unique region of parvovirus B19 and its constituent phospholipase A2-like activity. J. Virol. **76:**2014–2018.
18. **Dryden, K. A., G. Wang, M. Yeager, M. L. Nibert, K. M. Coombs, D. B. Furlong, B. N. Fields, and T. S. Baker.** 1993. Early steps in reovirus infection are associated with dramatic changes in supramolecular structure and protein conformation: analysis of virions and subviral particles by cryoelectron microscopy and image reconstruction. J. Cell Biol. **122:**1023–1041.
19. **Dubielzig, R., J. A. King, S. Weger, A. Kern, and J. A. Kleinschmidt.** 1999. Adeno-associated virus type 2 protein interactions: formation of preencapsidation complexes. J. Virol. **73:**8989–8998.
20. **Farr, G. A., and P. Tattersall.** 2004. A conserved leucine that constricts the pore through the capsid five-fold cylinder plays a central role in parvoviral infection. Virology **323:**243–256.
21. **Fujisawa, H., and M. Morita.** 1997. Phage DNA packaging. Genes Cells **2:** 537–545.
22. **Girod, A., C. E. Wobus, Z. Zadori, M. Ried, K. Leike, P. Tijssen, J. A. Kleinschmidt, and M. Hallek.** 2002. The VP1 capsid protein of adeno-associated virus type 2 is carrying a phospholipase A2 domain required for virus infectivity. J. Gen. Virol. **83:**973–978.
23. **Greber, U. F., and A. Fassati.** 2003. Nuclear import of viral DNA genomes. Traffic **4:**136–143.
24. **Grimm, D., A. Kern, M. Pawlita, F. Ferrari, R. Samulski, and J. Kleinschmidt.** 1999. Titration of AAV-2 particles via a novel capsid ELISA: packaging of genomes can limit production of recombinant AAV-2. Gene Ther. **6:**1322–1330.
25. **Guo, P.** 1994. Principles, perspectives and potential applications in viral assembly. Semin. Virol. **5:**27–37.
26. **Hansen, J., K. Qing, and A. Srivastava.** 2001. Adeno-associated virus type 2-mediated gene transfer: altered endocytic processing enhances transduction efficiency in murine fibroblasts. J. Virol. **75:**4080–4090.
27. **Hansen, J., K. Qing, and A. Srivastava.** 2001. Infection of purified nuclei by adeno-associated virus 2. Mol. Ther. **4:**289–296.
28. **Heilbronn, R., A. Burkle, S. Stephan, and H. zur Hausen.** 1990. The adeno-associated virus *rep* gene suppresses herpes simplex virus-induced DNA amplification. J. Virol. **64:**3012–3018.
29. **Hendrix, R. W.** 1998. Bacteriophage DNA packaging: RNA gears in a DNA transport machine. Cell **94:**147–150.
30. **Hewat, E. A., and D. Blaas.** 2004. Cryoelectron microscopy analysis of the structural changes associated with human rhinovirus type 14 uncoating. J. Virol. **78:**2935–2942.
31. **Hewat, E. A., E. Neumann, and D. Blaas.** 2002. The concerted conformational changes during human rhinovirus 2 uncoating. Mol. Cell **10:**317–326.
32. **Hirt, B.** 1967. Selective extraction of polyoma DNA from infected mouse cell cultures. J. Mol. Biol. **26:**365–369.
33. **James, J. A., C. R. Escalante, M. Yoon-Robarts, T. A. Edwards, R. M. Linden, and A. K. Aggarwal.** 2003. Crystal structure of the SF3 helicase from adeno-associated virus type 2. Structure **11:**1025–1035.
34. **Johnson, F. B., H. L. Ozer, and M. D. Hoggan.** 1971. Structural proteins of adenovirus-associated virus type 3. J. Virol. **8:**860–863.
35. **Kern, A., K. Schmidt, C. Leder, O. J. Muller, C. E. Wobus, K. Bettinger, C. W. Von der Lieth, J. A. King, and J. A. Kleinschmidt.** 2003. Identification of a heparin-binding motif on adeno-associated virus type 2 capsids. J. Virol. **77:**11072–11081.
36. **King, J. A., R. Dubielzig, D. Grimm, and J. A. Kleinschmidt.** 2001. DNA helicase-mediated packaging of adeno-associated virus type 2 genomes into preformed capsids. EMBO J. **20:**3282–3291.
37. **Kronenberg, S., J. A. Kleinschmidt, and B. Bottcher.** 2001. Electron cryomicroscopy and image reconstruction of adeno-associated virus type 2 empty capsids. EMBO Rep. **2:**997–1002.
38. **Laughlin, C. A., J. D. Tratschin, H. Coon, and B. J. Carter.** 1983. Cloning of infectious adeno-associated virus genomes in bacterial plasmids. Gene **23:** 65–73.
39. **Li, Y., Z. Zadori, H. Bando, R. Dubuc, G. Fediere, J. Szelei, and P. Tijssen.** 2001. Genome organization of the densovirus from Bombyx mori (BmDNV-1) and enzyme activity of its capsid. J. Gen. Virol. **82:**2821–2825.
40. **Llamas-Saiz, A. L., M. Agbandje-McKenna, W. R. Wikoff, J. Bratton, P. Tattersall, and M. G. Rossmann.** 1997. Structure determination of minute virus of mice. Acta Crystallogr. Sect. D **53:**93–102.
41. **Lombardo, E., J. C. Ramirez, J. Garcia, and J. M. Almendral.** 2002. Complementary roles of multiple nuclear targeting signals in the capsid proteins of the parvovirus minute virus of mice during assembly and onset of infection. J. Virol. **76:**7049–7059.
42. **McKenna, R., N. H. Olson, P. R. Chipman, T. S. Baker, T. F. Booth, J. Christensen, B. Aasted, J. M. Fox, M. E. Bloom, J. B. Wolfinbarger, and M. Agbandje-McKenna.** 1999. Three-dimensional structure of Aleutian mink disease parvovirus: implications for disease pathogenicity. J. Virol. **73:** 6882–6891.
43. **Meyer, W. J., S. Gidwitz, V. K. Ayers, R. J. Schoepp, and R. E. Johnston.** 1992. Conformational alteration of Sindbis virion glycoproteins induced by heat, reducing agents, or low pH. J. Virol. **66:**3504–3513.
44. **Moore, S. D., and P. E. Prevelige, Jr.** 2002. DNA packaging: a new class of molecular motors. Curr. Biol. **12:**96–98.
45. **Muzyczka, N., and K. I. Berns.** 2001. Parvoviridae: the viruses and their replication, p. 2327–2360. *In* D. M. Knipe and P. M. Howley (ed.), Fields virology, 4th ed. Lippincott Williams & Wilkins, Philadelphia, Pa.
46. **Myers, M. W., and B. J. Carter.** 1980. Assembly of adeno-associated virus. Virology **102:**71–82.
47. **Naldini, L., U. Blomer, P. Gallay, D. Ory, R. Mulligan, F. H. Gage, I. M. Verma, and D. Trono.** 1996. In vivo gene delivery and stable transduction of nondividing cells by a lentiviral vector. Science *2***72:**263–267.
48. **Newcomb, W. W., R. M. Juhas, D. R. Thomsen, F. L. Homa, A. D. Burch, S. K. Weller, and J. C. Brown.** 2001. The UL6 gene product forms the portal for entry of DNA into the herpes simplex virus capsid. J. Virol. **75:**10923–10932.
49. **Paradiso, P. R., S. L. Rhode, and I. I. Singer.** 1982. Canine parvovirus: a biochemical and ultrastructural characterization. J. Gen. Virol. **62:**113–125.
50. **Qing, K., C. Mah, J. Hansen, S. Zhou, V. Dwarki, and A. Srivastava.** 1999. Human fibroblast growth factor receptor 1 is a co-receptor for infection by adeno-associated virus 2. Nat. Med. **5:**71–77.
51. **Reguera, J., A. Carreira, L. Riolobos, J. M. Almendral, and M. G. Mateu.** 2004. Role of interfacial amino acid residues in assembly, stability, and conformation of a spherical virus capsid. Proc. Natl. Acad. Sci. USA **101:** 2724–2729.
52. **Reinisch, K. M., M. L. Nibert, and S. C. Harrison.** 2000. Structure of the reovirus core at 3.6 A resolution. Nature *4***04:**960–967.
53. **Ruffing, M., H. Heid, and J. A. Kleinschmidt.** 1994. Mutations in the carboxy terminus of adeno-associated virus 2 capsid proteins affect viral infectivity: lack of an RGD integrin-binding motif. J. Gen. Virol. **75:**3385–3392.
54. **Sanlioglu, S., P. K. Benson, J. Yang, E. M. Atkinson, T. Reynolds, and J. F. Engelhardt.** 2000. Endocytosis and nuclear trafficking of adeno-associated virus type 2 are controlled by Rac1 and phosphatidylinositol-3 kinase activation. J. Virol. **74:**9184–9196.
55. **Sayle, R. A., and E. J. Milner-White.** 1995. RASMOL: biomolecular graphics for all. Trends Biochem. Sci. **20:**374.
56. **Seisenberger, G., M. U. Ried, T. Endress, H. Buning, M. Hallek, and C. Brauchle.** 2001. Real-time single-molecule imaging of the infection pathway of an adeno-associated virus. Science *2***94:**1929–1932.
57. **Shi, W., G. S. Arnold, and J. S. Bartlett.** 2001. Insertional mutagenesis of the adeno-associated virus type 2 (AAV2) capsid gene and generation of AAV2 vectors targeted to alternative cell-surface receptors. Hum. Gene Ther. **12:** 1697–1711.
58. **Siegl, G., R. C. Bates, K. I. Berns, B. J. Carter, D. C. Kelly, E. Kurstak, and P. Tattersall.** 1985. Characteristics and taxonomy of Parvoviridae. Intervirology **23:**61–73.
59. **Simpson, A. A., P. R. Chipman, T. S. Baker, P. Tijssen, and M. G. Rossmann.** 1998. The structure of an insect parvovirus (Galleria mellonella densovirus) at 3.7 A resolution. Structure **6:**1355–1367.
60. **Smith, A. E., and A. Helenius.** 2004. How viruses enter animal cells. Science *3***04:**237–242.
61. **Srivastava, A., E. W. Lusby, and K. I. Berns.** 1983. Nucleotide sequence and organization of the adeno-associated virus 2 genome. J. Virol. **45:**555–564.
62. **Suikkanen, S., M. Antila, A. Jaatinen, M. Vihinen-Ranta, and M. Vuento.** 2003. Release of canine parvovirus from endocytic vesicles. Virology **316:** 267–280.
63. **Summerford, C., and R. J. Samulski.** 1998. Membrane-associated heparan sulfate proteoglycan is a receptor for adeno-associated virus type 2 virions. J. Virol. **72:**1438–1445.
64. **Summerford, C., J. S. Bartlett, and R. J. Samulski.** 1999. AlphaVbeta5 integrin: a co-receptor for adeno-associated virus type 2 infection. Nat. Med. **5:**78–82.
65. **Thomas, C. E., T. A. Storm, Z. Huang, and M. A. Kay.** 2004. Rapid uncoating of vector genomes is the key to efficient liver transduction with pseudotyped adeno-associated virus vectors. J. Virol. **78:**3110–3122.
66. **Tsao, J., M. S. Chapman, M. Agbandje, W. Keller, K. Smith, H. Wu, M. Luo, T. J. Smith, M. G. Rossmann, and R. W. Compans.** 1991. The three-dimen-

sional structure of canine parvovirus and its functional implications. Science **251:**1456–1464.
67. **Tullis, G. E., L. R. Burger, and D. J. Pintel.** 1992. The trypsin-sensitive RVER domain in the capsid proteins of minute virus of mice is required for efficient cell binding and viral infection but not for proteolytic processing in vivo. Virology **191:**846–857.
68. **Valpuesta, J. M., and J. L. Carrascosa.** 1994. Structure of viral connectors and their function in bacteriophage assembly and DNA packaging. Q. Rev. Biophys. **27:**107–155.
69. **Vihinen-Ranta, M., D. Wang, W. S. Weichert, and C. R. Parrish.** 2002. The VP1 N-terminal sequence of canine parvovirus affects nuclear transport of capsids and efficient cell infection. J. Virol. **76:**1884–1891.
70. **Vihinen-Ranta, M., S. Suikkanen, and C. R. Parris.** 2004. Pathways of cell infection by parvoviruses and adeno-associated viruses. J. Virol. **78:**6709–6714.
71. **Walters, R. W., M. Agbandje-McKenna, V. D. Bowman, T. O. Moninger, N. H. Olson, M. Seiler, J. A. Chiorini, T. S. Baker, and J. Zabner.** 2004. Structure of adeno-associated virus serotype 5. J. Virol. **78:**3361–3371.
72. **Warrington, K. H., O. S. Gorbatyuk, J. K. Harrison, S. R. Opie, S. Zolotukhin, and N. Muzyczka.** 2004. Adeno-associated virus type 2 VP2 capsid protein is nonessential and can tolerate large peptide insertions at its N terminus. J. Virol. **78:**6595–6609.
73. **Weger, S., A. Wistuba, D. Grimm, and J. A. Kleinschmidt.** 1997. Control of adeno-associated virus type 2 cap gene expression: relative influence of helper virus, terminal repeats, and Rep proteins. J. Virol. **71:**8437–8447.
74. **Weichert, W. S., J. S. Parker, A. T. Wahid, S. F. Chang, E. Meier, and C. R. Parrish.** 1998. Assaying for structural variation in the parvovirus capsid and its role in infection. Virology **250:**106–117.
75. **Whittaker, G. R.** 2003. Virus nuclear import. Adv. Drug Deliv. Rev. **55:**733–747.
76. **Wistuba, A., S. Weger, A. Kern, and J. A. Kleinschmidt.** 1995. Intermediates of adeno-associated virus type 2 assembly: identification of soluble complexes containing Rep and Cap proteins. J. Virol. **69:**5311–5319.
77. **Wistuba, A., A. Kern, S. Weger, D. Grimm, and J. A. Kleinschmidt.** 1997. Subcellular compartmentalization of adeno-associated virus type 2 assembly. J. Virol. **71:**1341–1352.
78. **Wobus, C. E., B. Hugle-Dorr, A. Girod, G. Petersen, M. Hallek, and J. A. Kleinschmidt.** 2000. Monoclonal antibodies against the adeno-associated virus type 2 (AAV-2) capsid: epitope mapping and identification of capsid domains involved in AAV-2–cell interaction and neutralization of AAV-2 infection. J. Virol. **74:**9281–9293.
79. **Wu, H., and M. G. Rossmann.** 1993. The canine parvovirus empty capsid structure. J. Mol. Biol. **233:**231–244.
80. **Wu, P., W. Xiao, T. Conlon, J. Hughes, M. Agbandje-McKenna, T. Ferkol, T. Flotte, and N. Muzyczka.** 2000. Mutational analysis of the adeno-associated virus type 2 (AAV2) capsid gene and construction of AAV2 vectors with altered tropism. J. Virol. **74:**8635–8647.
81. **Xia, Q., J. Jakana, J. Q. Zhang, and Z. H. Zhou.** 2003. Structural comparisons of empty and full cytoplasmic polyhedrosis virus. Protein-RNA interactions and implications for endogenous RNA transcription mechanism. J. Biol. Chem. **278:**1094–1100.
82. **Xiao, W., K. H. Warrington, Jr., P. Hearing, J. Hughes, and N. Muzyczka.** 2002. Adenovirus-facilitated nuclear translocation of adeno-associated virus type 2. J. Virol. **76:**11505–11517.
83. **Xie, Q., and M. S. Chapman.** 1996. Canine parvovirus capsid structure, analyzed at 2.9 A resolution. J. Mol. Biol. **264:**497–520.
84. **Xie, Q., W. Bu, S. Bhatia, J. Hare, T. Somasundaram, A. Azzi, and M. S. Chapman.** 2002. The atomic structure of adeno-associated virus (AAV-2), a vector for human gene therapy. Proc. Natl. Acad. Sci. USA **99:**10405–10410.
85. **Yuan, W., and C. R. Parrish.** 2001. Canine parvovirus capsid assembly and differences in mammalian and insect cells. Virology **279:**546–557.
86. **Zadori, Z., J. Szelei, M. C. Lacoste, Y. Li, S. Gariepy, P. Raymond, M. Allaire, I. R. Nabi, and P. Tijssen.** 2001. A viral phospholipase A2 is required for parvovirus infectivity. Dev. Cell **1:**291–302.
87. **Zolotukhin, S., M. Potter, I. Zolotukhin, Y. Sakai, S. Loiler, T. J. Fraites, Jr., V. A. Chiodo, T. Phillipsberg, N. Muzyczka, W. W. Hauswirth, T. R. Flotte, B. J. Byrne, and R. O. Snyder.** 2002. Production and purification of serotype 1, 2, and 5 recombinant adeno-associated viral vectors. Methods **28:**158–167.